Available online at www.sciencedirect.com
SCIENCE DIRECT
ELSEVIER
Ultramicroscopy 106 (2006) 614–619
ultramicroscopy
www.elsevier.com/locate/ultramic

Magnetisation reversal in epitaxial Fe(1 0 0) disks studied by high resolution scanning Hall probe microscopy

J.S. Neal[a,*], H.G. Roberts[a], M.R. Connolly[a], S. Crampin[a], S.J. Bending[a], G. Wastlbauer[b], J.A.C. Bland[b]

[a]*Department of Physics, University of Bath, Bath BA2 7AY, UK*
[b]*Department of Physics, University of Cambridge, Cambridge CB3 0HE, UK*

Received 25 October 2005; received in revised form 1 February 2006; accepted 9 March 2006

Abstract

Magnetisation reversal has been investigated in 2 μm diameter epitaxial Fe(1 0 0) disks using scanning Hall probe microscopy. The high spatial resolution (~200 nm) and non-invasiveness of our Hall sensors has allowed the domain structure, which is governed by biaxial in-plane anisotropy, to be resolved in the disks. We find that most disks appear to exhibit a *double vortex* magnetisation reversal mechanism, in agreement with the results of micromagnetic simulations with the OOMMF code. Although the switching dynamics tend to be influenced by domain wall pinning sites within our Fe samples, we find a strong correlation between most of our measured images and the results of simulations. Additional confirmation for the double vortex reversal mechanism is drawn from local measurements of out-of-plane magnetic induction loops.

PACS: 75.60.Jk; 75.60.Ch; 75.50.−y; 07.79.−v

Keywords: Hall sensors; Epitaxial iron thin films; Ferromagnetic domains; Magnetisation reversal

A detailed understanding of the magnetisation reversal process and domain structures present in ferromagnetic thin films and nanostructures is essential for the realisation of applications in data storage and magnetoelectronic devices. The magnetic force microscope [1] (MFM) is currently the instrument of choice for high spatial resolution domain imaging, but suffers from a number of limitations. The magnetic tip can be invasive and has a micromagnetic state which is rarely known with any confidence and may change in an applied magnetic field. In addition the technique maps gradients in the magnetic force rather than magnetisation or magnetic induction directly, making quantitative interpretation difficult. Hence MFM is poorly suited to studies of magnetisation reversal and is primarily used to image remnant states. Several other scanning probe techniques have been developed in recent years to address some of these problems including scanning SQUID microscopy [2], scanning magnetoresistive sensors [3] and scanning Hall probe microscopy [4–7] (SHPM). Of these SHPM seems to have the greatest promise since the Hall sensors are non-invasive and provide quantitative information about the out-of-plane component of magnetic induction which can be compared directly with the results of micromagnetic simulations. The technique also allows one to image the domain structure of a sample at *any arbitrary point* on the magnetisation hysteresis cycle as well as generate 'local' *M–H* loops at selected spatial locations. Several recent studies have demonstrated that SHPM is capable of imaging domain reversal in ferromagnetic thin films [8] and patterned microstructures [9]. We demonstrate here that very high resolution Hall sensors can also be used to map the *nanoscale* domain structure of micron-sized ferromagnetic disks during magnetisation reversal.

The flux closure vortex state in micron-sized ferromagnetic disks [10] and rings [11] has attracted considerable interest over the last decade, both from fundamental

*Corresponding author. Tel.: +44 1255 38 3626; fax: +44 1255 38 6110.
E-mail address: j.s.neal@bath.ac.uk (J.S. Neal).

0304-3991/$ - see front matter © 2006 Elsevier B.V. All rights reserved.
doi:10.1016/j.ultramic.2006.03.002

physics considerations as well as for potential data storage applications [12]. To date mostly polycrystalline rings/disks without pronounced anisotropy have been studied, and it is important to extend these investigations to epitaxial disks, when the anisotropy will strongly influence vortex-like states formed. Epitaxial iron thin films have been extensively studied in recent years since it was demonstrated that it is possible to inject spin-polarised electrons from them into GaAs [13] and AlGaAs [14]. However, the effect of the strong magnetocrystalline anisotropy on the magnetisation reversal process is still not fully understood (a detailed review of this subject is given in Ref. [15]). Previous studies [16–18] of the epitaxial Fe/GaAs system have led to an understanding of the interplay between interface effects, film thickness and lateral dimensions. Epitaxial Fe (0 0 1) films with thicknesses greater than 2 nm exhibit a biaxial anisotropy [18] aligned along the [1 0 0] and [0 1 0] axes, as found in bulk Fe. This magnetocrystalline anisotropy should reduce the effect of defects on the magnetisation reversal process compared to polycrystalline materials, and allow the formation of magnetic structures with more predictable and reproducible properties. In epitaxial Fe microstructures the anisotropy will cause the flux closure domains, formed to minimise magnetostatic energy, to have their magnetisations pointing along the magnetic easy axes of the film.

In this paper we report the results of SHPM and Hall magnetometry performed on an array of 2 μm Fe (1 0 0) disks grown epitaxially on a pre-patterned GaAs (1 0 0) substrate. Initially electron beam lithography was used to define a square array of 2 μm diameter disks with a lattice spacing of 6 μm. This mask was then dry etched into the GaAs to a depth of ~100 nm and the resist removed, leaving an array of free-standing GaAs pillars. A 20 nm Fe film was then grown by molecular beam epitaxy at room temperature over the entire sample and capped with 3 nm Cr and 10 nm Au layers. This procedure creates an array of epitaxial Fe disks on top of the pillars and, in principle, also allows the use of elevated deposition temperatures, which would not be possible if the sample was masked with resist. Previously [19] it has been shown that if the ratio of the disk separation to disk diameter is greater than unity, as is the case in our experiments, the disks will behave as isolated elements.

The results presented in this paper were obtained with a commercial scanning Hall probe microscope [5] fitted with a custom-fabricated GaAs/AlGaAs heterostructure two-dimensional electron gas Hall sensor (Fig. 1(a)) incorporating an integrated scanning tunnelling microscope (STM) tip formed by coating the corner of an etched mesa with a thin layer of gold. Hall bars with wire widths ~450 nm were fabricated using e-beam lithography and wet chemical etching. The top left inset in Fig. 2 shows an atomic force micrograph of the Hall bars and a cross section of the active Hall area, with a measured full width at half maximum of ~450 nm. This gives an effective electrical width of $\leqslant$250 nm after edge wall depletion of $\geqslant$100 nm,

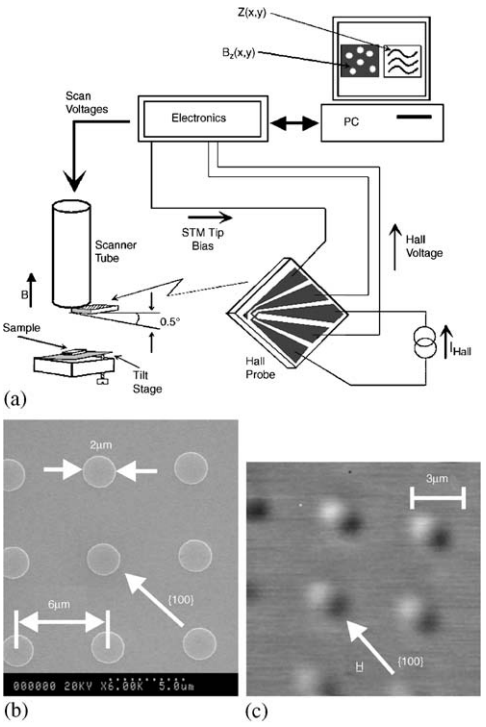

Fig. 1. (a) A schematic diagram of our scanning Hall probe microscope system. (b) A scanning electron microscope image of a section of the Fe disk array. (c) A 13 μm × 13 μm SHPM image of the Fe disk array at $T = 80$ K in a +740 Oe applied field applied along ⟨1 0 0⟩.

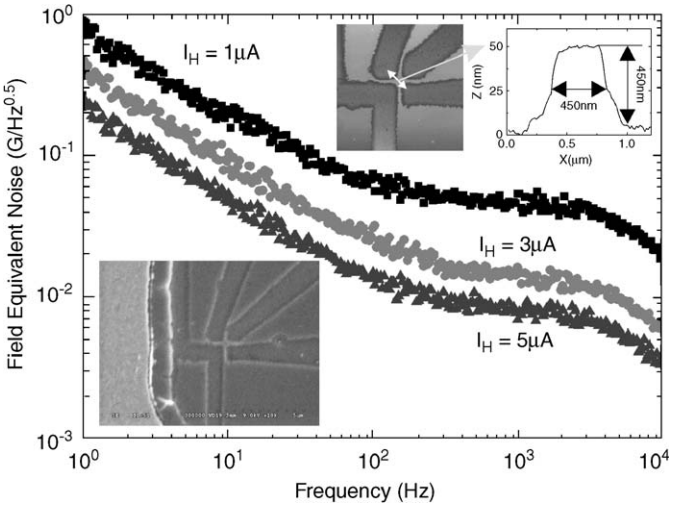

Fig. 2. Spectrum of the field equivalent noise (FEN) of the Hall sensor for Hall currents of 1, 3, and 5 μA, respectively, at 77 K. Bottom inset shows a scanning electron micrograph of the active area of the Hall sensor. Top inset (left) shows an atomic force micrograph of the Hall bars, along with a cross section profile (right) of the active area.

and a Hall coefficient R_H~0.3 Ω G^{-1} at 77 K. The packaged probe was screwed onto the end of the piezoelectric scanner tube of the scanning probe microscope. The GaAs substrate supporting the Fe disk array was stuck onto a separate sample puck, which was tilted $<0.5^\circ$ with

respect to the Hall probe to ensure that the STM tip (situated at the corner of the chip, about 5 μm away from the Hall probe) was always the closest point to the sample, and brought into tunnelling contact with a 'stick-slip' inertial approach mechanism. All of the results presented in this paper were obtained using a Hall current of $I_H = 4\,\mu A$, a measurement bandwidth of 100 Hz and a voltage gain of 1×10^4. High-resolution imaging was achieved by retracting the Hall sensor out of tunnelling contact so that it scanned in a parallel plane ~200 nm above the highest point of the sample. The field equivalent noise ((FEN = $V_n/(R_H I_H)$) of the Hall sensor measured at several operating currents is shown in Fig. 2. As expected [5] there are two principal components to the noise spectrum. At low frequencies the noise has a $1/f$ dependence with a corner frequency, f_c, of ~100 Hz. At higher frequencies the noise spectrum is dominated by white Johnson noise ($V_J = \sqrt{4kTR_V\Delta f}$ where R_V is the series resistance of the voltage leads and Δf the measurement bandwidth). Above ~2 kHz the noise voltage rolls off due to the measurement bandwidth of the pre-amplifier used (~10 kHz for noise measurements). The noise sources in the Hall bar were suppressed by cooling both sample and sensor to 80 K using a temperature-controlled liquid nitrogen cryostat.

The external magnetic field was supplied by a modified commercial electromagnet, capable of providing fields up to ±740 Oe in any direction in the plane of the sample. The images and local induction loops shown here were all taken with the magnetic field applied in-plane along one of the ⟨1 0 0⟩ easy axes of the Fe film.

Fig. 1 shows a scanning electron micrograph (Fig. 1(b)) and an SHPM image (Fig. 1(c), taken at saturation magnetisation with the applied field along ⟨1 0 0⟩) of a relatively large region of the sample. The pre-patterning technique has the disadvantage, however, that a commensurate array of antidots is simultaneously formed 100 nm below the disks whose magnetisation behaviour must be distinguished in imaging experiments. In practice this can be achieved relatively easily for two reasons. If we scan at a constant height above the sample we are always much more sensitive (approximately exponentially so) to the Fe disks which are 100 nm closer to the Hall sensor. In addition the antidot film has a rather small coercive field (~50 Oe) and switches very abruptly at 80 K in comparison to the disks.

Fig. 3 shows the typical evolution of the domain structure of a single Fe disk as the in-plane magnetic field is varied from −740 to +740 Oe and back again. The clear dipole contrast observed at both positive and negative maximum applied fields (Figs. 3(a) and (h)) indicates that the disk is close to saturation magnetisation. Starting at negative saturation and moving around the magnetisation curve we find almost no change in the images (apart from a slight clockwise rotation of the dipole) until the applied field is reversed to ~+50 Oe (Fig. 3(b)). At this field local induction loops anywhere above the sample show a sharp spike and the image contrast (as indicated by the greyscale (GS), the ($B_z^{max} - B_z^{min}$) field span assigned to the 8-bit grey

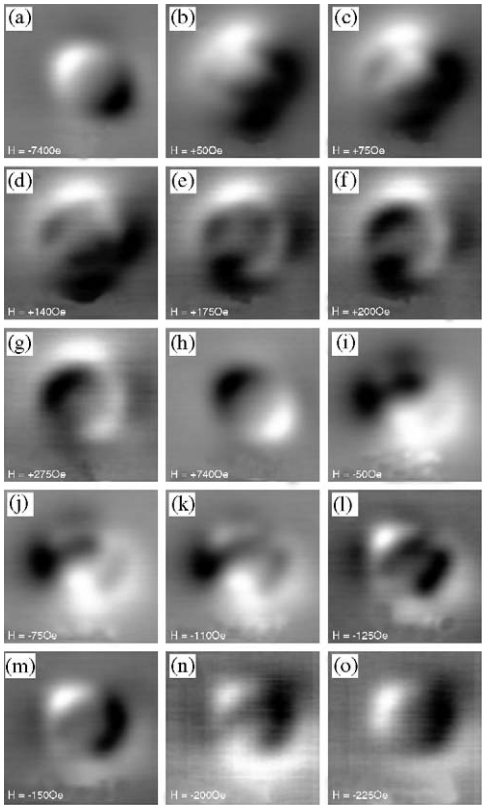

Fig. 3. Typical SHPM images of a single Fe disk at $T = 80$ K in various applied fields (image sizes all 4 μm × 4 μm). (a) $H = -740$ Oe (greyscale (GS)~11.02 G), (b) $H = +50$ Oe (GS~19.6 G), (c) $H = +75$ Oe (GS~16.47 G), (d) $H = +140$ Oe (GS~9.7 G), (e) $H = +175$ Oe (GS~8.04 G), (f) $H = +200$ Oe (GS~7.39 G), (g) $H = +275$ Oe (GS~7.76 G), (h) $H = +740$ Oe (GS~10.22 G), (i) $H = -50$ Oe (GS~15.82 G), (j) $H = -75$ Oe (GS~14.28 G), (k) $H = -110$ Oe (GS~12.74 G), (l) $H = -125$ Oe (GS~7.34 G), (m) $H = -150$ Oe (GS~11 G), (n) $H = -200$ Oe (GS~4.27 G), and (o) $B = -225$ Oe (GS~4.72 G).

palette between white and black in the caption to Fig. 3) suddenly jumps to a maximum, indicating that the antidot film has abruptly reversed its magnetisation state. Any changes in the images beyond this point can be associated with changes to the Fe disks and, as expected, we find a gradual reduction in image contrast (greyscale) as positive saturation is approached. While different disks switched configurations at slightly different applied fields, most showed approximately the same structural evolution. Detailed examination of our images indicates the presence of a rather complex domain structure which is not consistent with the 4 domain flux closure 'vortex-like' structure which we were expecting and had been seen previously in similar *AC demagnetised* epitaxial (0 0 1) ferromagnetic disks [20]. To understand the magnetisation process micromagnetic simulations were performed using the Object Orientated Micromagnetics Framework (OOMMF) from NIST [21]. Calculations were performed for 2 μm diameter disks using an exchange constant of [18,20] $A = 2.1 \times 10^{-11}\,J\,m^{-1}$, a cubic anisotropy constant of [18,20] $K_1 = 4.8 \times 10^4\,J\,m^{-3}$ and a saturation

magnetisation value of $M_s = 1.7 \times 10^6\,\mathrm{A\,m^{-1}}$. The chosen mesh size for the calculations was 5 nm, this was selected for accuracy and computational convenience. The suitability of the 5 nm mesh size was ascertained by testing various mesh sizes for convergence and ensuring they all exhibited similar qualitative results. The external field was applied along one of the in-plane easy axis and varied in discrete steps between −750 and +750 Oe. The simulation was run forwards and backwards through this field range several times before results were taken to eliminate any dependence on initial conditions.

The simulated domain structures (Fig. 4) for the Fe disks show the presence of a 7 domain 'double' vortex reversal mechanism [22]. The symmetry of the magnetisation reversal process present in the Fe disks means the simulated results are not unique. Hence, each vortex can nucleate in one of two places and can have clockwise or anti-clockwise vorticity. However, once one vortex has nucleated with a specific vorticity the location and vorticity of the second vortex is fixed in the lowest energy configuration. The simulations are biased towards a preferred state, to allow reproducible results to be collected, and when attempting to correlate simulations and images the four possible starting conditions must be considered. The simulations show that the vortex cores enter the sample at either side of the (saturation) poles, and then proceed to move to the other side of the pole and exit midway between poles. During this process a large central domain is formed with magnetisation perpendicular to the applied field, which increases in size and then shrinks again as the vortex cores move. From the simulations we see that the double vortex mechanism is intrinsically frustrated and cannot provide optimal flux closure for all of the domain walls. 'Compromise' domain walls are clearly visible as regions of strong contrast in our images. The simulations also reveal that the moments near the disk edges are rotated away from the easy axes and tend to become parallel to the edges of the disk in order to reduce the magnetostatic energy of the system.

To compare the simulated domain structure directly with our measurements we have used the output of the OOMMF code to calculate the perpendicular component of magnetic field at a typical scanning height (~200 nm) above the disk. The antidot film was also included assuming that it was in a saturation magnetisation state whose direction was flipped as appropriate at the ±50 Oe switching field. This was then included in the model by adding the stray field of a disk of reversed magnetisation situated 100 nm further below the Hall sensor. Five distinct experimental configurations illustrated in Fig. 3 can be

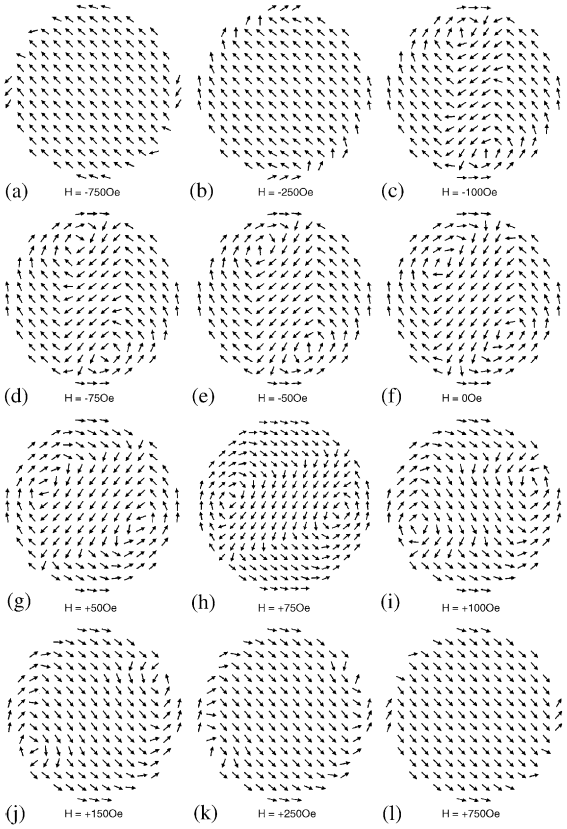

Fig. 4. Results of OOMMF simulations for a 2 μm diameter Fe disk at various applied fields applied along ⟨1 0 0⟩ (see text for details). (a) $H = -750$ Oe, (b) $H = -250$ Oe, (c) $H = -100$ Oe, (d) $H = -75$ Oe, (e) $H = -50$ Oe, (f) $H = 0$ Oe, (g) $H = 50$ Oe, (*h*)$H = 75$ Oe, (i) $H = 100$ Oe, (j) $H = 150$ Oe, (k) $H = 250$ Oe, (l) $H = 750$ Oe.

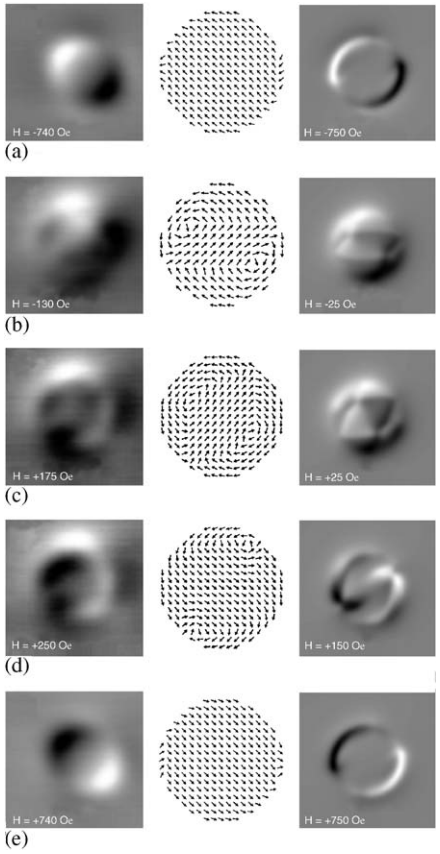

Fig. 5. Comparison between experimental SHPM images and the results of OOMMF simulations at several applied magnetic fields.

quite successfully identified with specific domain simulations as shown in Fig. 5. In practice the correlation is not perfect for a number of reasons; the experimental images are distorted by domain wall pinning (for the same reason the experimental and simulation applied fields also differ considerably), and the finite (~200 nm) resolution of the Hall probe has not been taken into account. Nevertheless, a number of common features, e.g. the white/black triangular contrast at the centre of Fig. 5(c) are quite compelling evidence for the proposed double vortex nucleation mechanism.

Local out-of-plane magnetic inductance loops taken at various sites on the same disk provide additional confirmation of the reversal mechanism. The experimental $B_z(H)$ curves shown in Fig. 6 were obtained by parking the Hall sensor at fixed locations above the disk (indicated by the black dots on the SHPM image) and recording the Hall voltage while sweeping the applied in-plane field between positive and negative saturation. The duration of each sweep was fixed at 60 s and each sweep was averaged 5 times to improve signal to noise ratios.

A set of simulated $B_z(H)$ curves was also generated (Fig. 7) at the same strategic points on the disk which included vortex nucleation and annihilation points. In order to best account for the presence of the antidot array this had to be done in a slightly contrived way. In all cases the background antidot array was assumed to have already switched into saturation, even at the most negative applied fields simulated. In this way we are able to compare the qualitative shape of the 'curves' with the experimental data for increasing fields beyond the switching point of the antidot array (i.e. $H > +50$ Oe), however for the reasons detailed above, the simulated transition fields do not coincide with those observed experimentally. Note that the presence of a sharp spike at $\sim +50$ Oe present in all of the experimental curves, which is attributed to the abrupt reversal of the antidot film, is consequently not reproduced in the simulations. Overlooking this feature we find a strong qualitative similarity between experimental and

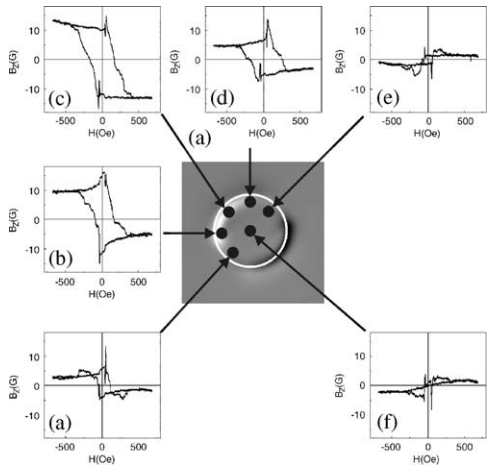

Fig. 6. Experimental $B_z(H)$ hysteresis loops measured above the indicated positions on the Fe disk.

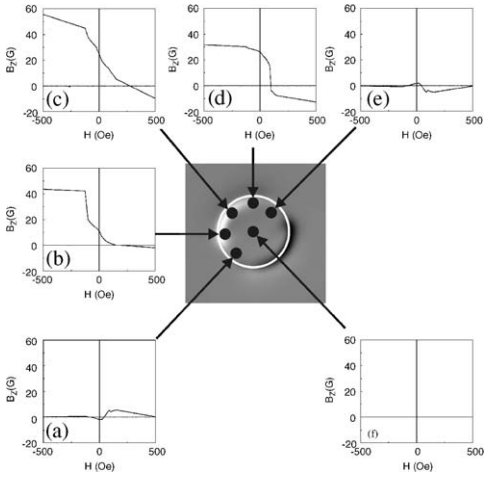

Fig. 7. Simulated $B_z(H)$ hysteresis loops at the indicated locations on the Fe disk (see text for the protocol used).

theoretical curves. The relative amplitudes of the experimental curves map onto the relative amplitudes of the simulated curves in all cases, being maximum near the poles and minimum along a line halfway between the poles and perpendicular to the magnetic field. There are also similarities between the structures of the curves; for example the step/shoulder structures in Figs. 6(b)–(d) correspond quite closely to similar features in the simulations (Figs. 7(b)–(d)). The measured induction at the centre of the disk (Fig. 6(f)) is close to the zero value predicted by the simulation (Fig. 7(f)) for a symmetrical double vortex structure. The fact that it is not exactly zero is either due to symmetry breaking caused by domain wall pinning in the disk or slight mispositioning of the Hall sensor. Finally the curves measured in Figs. 6(a) and (e) both have local induction peaks which are greater in magnitude than in the saturation magnetisation state in a manner reminiscent of the simulations, although the overall background hysteresis is again much stronger than the model predicts for the reasons indicated in the previous sentence.

In conclusion, we have used very high resolution SHPM to investigate the magnetisation reversal processes of 2 μm diameter epitaxial Fe disks grown on (1 0 0) GaAs. Images of the out-of-plane component of the demagnetising field of the disk array were captured as a function of applied field. These were interpreted by direct comparison with micromagnetic simulations performed using the OOMMF code, which was adapted to generate greyscale induction images and local induction loops for the disks. The simulations predicted the presence of a 7 domain 'double vortex' magnetisation reversal process driven by the biaxial magnetic anisotropy. A direct comparison with magnetic images and local induction loops at strategic points on the disk lends quite strong support to this double vortex magnetisation reversal mechanism.

We acknowledge the support of EPSRC studentship number GR/P02707/01 and Grant number GR/R18413/01.

We also thank Dr. Carlos Vaz for proof-reading the manuscript.

References

[1] Y. Martin, H.K. Wickramasinghe, Appl. Phys. Lett. 50 (1987) 1455.
[2] J.R. Kirtley, M.B. Ketchen, K.G. Stawiasz, J.Z. Sun, W.J. Gallagher, S.H. Blanton, S.J. Wind, Appl. Phys. Lett. 66 (1995) 1138.
[3] R. O'Barr, M. Lederman, S. Schultz, J. Appl. Phys. 79 (1996) 6067.
[4] A.M. Chang, H.D. Hallen, L. Harriot, H.F. Hess, H.L. Loa, J. Kao, R.E. Miller, T.Y. Chang, Appl. Phys. Lett. 61 (1992) 1974.
[5] A. Oral, S.J. Bending, M. Henini, Appl. Phys. Lett. 69 (1996) 1324.
[6] T. Schweinbock, D. Weiss, M. Lipinski, K. Eberl, J. Appl. Phys. 87 (2000) 6496.
[7] A. Sandhu, K. Kurosawa, M. Dede, A. Oral, Jpn. J. Appl. Phys. 43 (1) (2004) 777.
[8] G.D. Howells, A. Oral, S.J. Bending, S.R. Andrews, P.T. Squire, P. Rice, A. de Lozanne, J.A.C. Bland, I. Kaya, M. Henini, J. Magn. Magn. Mater. 196–197 (1999) 917;
A. Sandhu, H. Masuda, A. Oral, S.J. Bending, Jpn. J. Appl. Phys. 40 (2001) 4321;
A. Sandhu, N. Iida, H. Masuda, A. Oral, S.J. Bending, J. Magn. Magn. Mater. 242 (2002) 1249;
A. Sandhu, H. Masuda, A. Oral, Jpn. J. Appl. Phys. 41 (2002) L1402.
[9] J. Bekaert, D. Buntix, C. Van Haesendonck, V.V. Moshchalkov, J. De Boeck, G. Borghs, V. Metlushko, Appl. Phys. Lett. 81 (2002) 3413.
[10] C.A.F. Vaz, L. Lopez-Diaz, M. Kläui, J.A.C. Bland, T.L. Monchesky, J. Unguris, Z. Cui, Phys. Rev. B 67 (2003) 140405(R).
[11] J. Rothman, M. Klaui, L. Lopez-Diaz, C.A.F. Vaz, A. Bleloch, J.A.C. Bland, Z. Cui, R. Speaks, Phys. Rev. Lett. 86 (2001) 1098.
[12] P. Vavassori, M. Grimsditch, V. Metlushko, N. Zaluzek, B. Ilic, Appl. Phys. Lett. 86 (2005) 072507.
[13] H.J. Zhu, et al., Phys. Rev. Lett. 87 (2001) 016601.
[14] A.T. Hanbicki, et al., Appl. Phys. Lett. 80 (2002) 1240.
[15] G. Wastlbauer, J.A.C. Bland, Adv. Phys. 54 (2005) 83.
[16] E. Gu, E. Ahmad, S.J. Gray, C. Daboo, J.A.C. Bland, L.M. Brown, M. Ruhrig, A.J. McGibbon, J.N. Chapman, Phys. Rev. Lett. 78 (1997) 1158.
[17] Y.B. Xu, A. Hirohata, L. Lopez-Diaz, H.T. Leung, M. Tselepi, S.M. Gardiner, W.Y. Lee, J.A.C. Bland, F. Rousseaux, E. Cambaril, H. Launois, J. Appl. Phys. 87 (2000) 7019.
[18] R. Pulwey, M. Zölfl, G. Bayreuther, D. Weiss, J. Appl. Phys. 93 (2003) 7432.
[19] A.O. Adeyeye, J.A.C. Bland, C. Daboo, D.G. Hasko, Phys. Rev. B 56 (1997) 3265.
[20] R. Pulwey, M. Zölfl, G. Bayreuther, D. Weiss, J. Appl. Phys. 91 (2002) 7995.
[21] M.J. Donahue, D.G. Porter, OOMMF User's Guide, Version 1.0., Interagency Report NISTIR 6376. National Institute of Standards and Technology, Gaithersburg, MD, September 1999 (http://math.nist.gov/oommf/).
[22] I.L. Prejebeanu, M. Natali, L.D. Buda, U. Ebels, A. Lebib, Y. Chen, K. Ounadjela, J. Appl. Phys. 91 (2002) 7343.